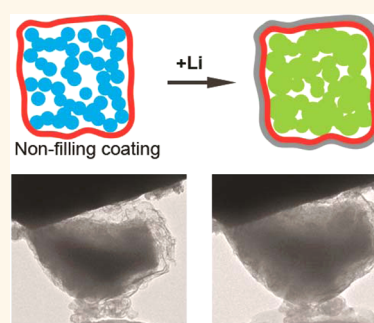# Nonfilling Carbon Coating of Porous Silicon Micrometer-Sized Particles for High-Performance Lithium Battery Anodes

Zhenda Lu,[†,§] Nian Liu,[†,§] Hyun-Wook Lee,[†] Jie Zhao,[†] Weiyang Li,[†] Yuzhang Li,[†] and Yi Cui*,[†,‡]

[†]Department of Materials Science and Engineering, Stanford University, Stanford, California 94305, United States and [‡]Stanford Institute for Materials and Energy Sciences, SLAC National Accelerator Laboratory, 2575 Sand Hill Road, Menlo Park, California 94025, United States. [§]Z. Lu and N. Liu contributed equally to this work.

ABSTRACT Silicon is widely recognized as one of the most promising anode materials for lithium-ion batteries due to its 10 times higher specific capacity than graphite. Unfortunately, the large volume change of Si materials during their lithiation/delithiation process results in severe pulverization, loss of electrical contact, unstable solid—electrolyte interphase (SEI), and eventual capacity fading. Although there has been tremendous progress to overcome these issues through nanoscale materials design, improved volumetric capacity and reduced cost are still needed for practical application. To address these issues, we design a nonfilling carbon-coated porous silicon microparticle (nC-pSiMP). In this structure, porous silicon microparticles (pSiMPs) consist of many interconnected primary silicon nanoparticles; only the outer surface of the pSiMPs was coated with carbon, leaving the interior pore structures unfilled. Nonfilling carbon coating hinders electrolyte penetration into the nC-pSiMPs, minimizes the electrode—electrolyte contact area, and retains the internal pore space for Si expansion. SEI formation is mostly limited to the outside of the microparticles. As a result, the composite structure demonstrates excellent cycling stability with high reversible specific capacity ($\sim$1500 mAh g^{-1}, 1000 cycles) at the rate of C/4. The nC-pSiMPs contain accurate void space to accommodate Si expansion while not losing packing density, which allows for a high volumetric capacity ($\sim$1000 mAh cm^{-3}). The areal capacity can reach over 3 mAh cm^{-2} with the mass loading 2.01 mg cm^{-2}. Moreover, the production of nC-pSiMP is simple and scalable using a low-cost silicon monoxide microparticle starting material.

Non-filling coating +Li

KEYWORDS: Si anodes · nonfilling coating · porous silicon microparticles

Intense academic and industrial effort has been devoted to developing rechargeable lithium-ion batteries with high energy density, long cycle life, and low cost for various technological applications, including portable electronics, electric vehicles, and grid-scale energy storage systems.[1−4] Surface coatings on electrode materials are effective ways to improve the battery performance by both enhancing the electronic conductivity and minimizing the electrode/electrolyte interfacial side reaction.[5−8] Conformal coatings are highly desired for this purpose, because uncoated areas remain vulnerable to attack by the electrolyte, compromising the functionality of the protection layer. However, for materials with large volume change, it is challenging to realize a stable coating since a large volume change ruptures the coating.

Silicon is regarded as one of the most promising anode materials for next-generation lithium-ion batteries due to its 10 times higher specific capacity than the existing graphite anodes.[9−12] However, silicon experiences large volume changes (up to 4 times) during the lithiation and delithiation processes. This volume change not only leads to rapid particle pulverization and isolation but also makes it difficult to coat a stable protection layer to maintain the solid—electrolyte interphase (SEI). The accumulated SEI eventually blocks the transport of Li$^+$ and e$^-$, causing the cell to fail.[13−15] Significant progress has been achieved to address these issues by combining a conformal coating with internal void space.[16] For example, double-walled Si nanotubes,[17] Si—C yolk shell nanostructures,[18−21] and pomegranate-like Si structures[22] have been
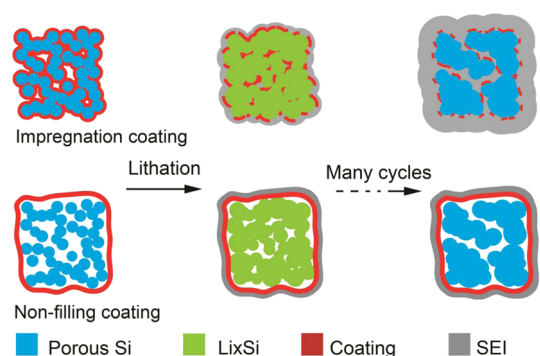
Figure 1. Schematic of coating design on mesoporous Si microparticles (pSiMPs) and their structural evolution during cycling. For impregnation coating, a carbon layer is coated on each of the Si nanoparticle domains. Upon first cycling, the tremendous volume expansion of Si domains breaks the coating, exposing the silicon surface to the electrolyte, and resulting in excessive SEI formation. For a nonfilling coating, however, carbon only coats the outside of the microparticle, leaving the internal void space for Si expansion. Upon (de)lithiation, the outer carbon layer remains intact. As a result, the SEI outside the microstructure is not ruptured during cycling and remains thin.

reported to substantially improve the cycling life of Si-based anodes. However, these core—shell structures with void space were all based on Si nanostructures, which introduce new challenges to the practical application of Si batteries.[23—29] First, the nanostructured materials are sparsely packed, making it difficult to achieve robust electronic and ionic connections between neighboring nanoparticles. Thus, high mass loading of active materials and high volumetric capacity remain challenging. There are only a few examples to address these issues with promise.[20,22] Second, most nanostructures require expensive and multistep synthesis. For example, silicon nanoparticles are produced by pyrolysis of silane gas, while the well-designed void space is introduced using a sacrificial template. The existing Si nanostructures are still too expensive for large-scale use.

To address these concerns, here we design a nonfilling carbon-coated porous Si microparticle (nC-pSiMP) core—shell structure as anode material. The core is a porous Si microparticle composed of interconnected Si primary nanoparticles,[30,31] and the shell is a confining carbon layer that allows Li$^+$ to pass through. No carbon exists in the pore space of Si, which is different from all the previous demonstrations in the literature, where the carbon coating penetrates into the structures.[32—37] Such a design offers multiple attractive features for large-volume-change anode materials: (1) a commercially available SiO microparticle source and a simple synthesis procedure make the process highly cost-effective and scalable. (2) The interconnected Si primary nanoparticles formed by thermal disproportionation of SiO microparticles ensures the size of the primary Si building blocks is less than 10 nm (Figure 2d, Supporting Information),[36,38—40]

which is below the critical fracture size.[41,42] Thermal disproportionation also results in densely packed primary Si nanoparticles, which allow for good electronic conductivity among neighboring particles. (3) Carbon coats the exterior surface of the Si microparticles, prevents electrolyte diffusion into the interior pore space, and restricts SEI formation to the outer surface. (4) The nonfilling coating retains enough internal void space to accommodate the volume expansion of Si nanoparticles and keeps the carbon shell intact during the electrochemical cycling (Figure 1). (5) The nonfilling coating introduces less carbon to the composites, which not only increases specific capacity but also increases the initial Coulombic efficiency due to Li trapping in amorphous carbon.

RESULTS

Material Synthesis and Characterization. Commercially available SiO microparticles were first conformally coated with a layer of resorcinol-formaldehyde resin (RF) in diluted ammonia aqueous solution.[43] Then the coated structures were heated to 950 °C for 5 h under Ar. During the heating process, phase separation in SiO occurs to form interconnected Si nanoparticles embedded in a SiO$_2$ matrix due to the thermal disproportionation of SiO.[36,39] Simultaneously, the RF coating was converted to a carbon coating at high temperature to wrap the as-formed Si/SiO$_2$ composites. After removing the SiO$_2$ matrix with HF solution, enough void space was generated to allow Si free expansion without breaking the outer carbon layer. This synthesis approach has three advantages. First, the chemical sources used in the synthesis (SiO microparticle, resorcinol, formaldehyde, ammonia, and HF) are all used industrially with low cost, providing great promise for mass production. Second, the carbon conversion and SiO thermal disproportionation are achieved in one heating step, saving energy during the preparation process. Third and most importantly, void space is formed by SiO disproportionation and HF etching without any intentionally added templates. The void space volume is sufficient for Si expansion, as evidenced by the *in situ* TEM results shown in Figure 4.

For a clear comparison of structure morphology, we prepared porous silicon microparticles with different carbon coatings: no coating, impregnating coating, and nonfilling coating, simplified as pSiMP, iC-SiMP, and nC-SiMP, respectively (Figure 2a—c). Representative TEM and SEM images are shown in Figure 2d—i. Without a carbon coating, one can easily observe the porous nature of the microparticles in TEM (Figure 2d) and the enlarged SEM images in the inset (Figure 2g). The interconnected Si nanoparticles are very uniform, with most less than 10 nm. For iC-SiMPs, the porous nature of the microparticles is not obvious in Figure 2e and h because of the carbon penetration into the interior pore space. For the nonfilling coated structure,
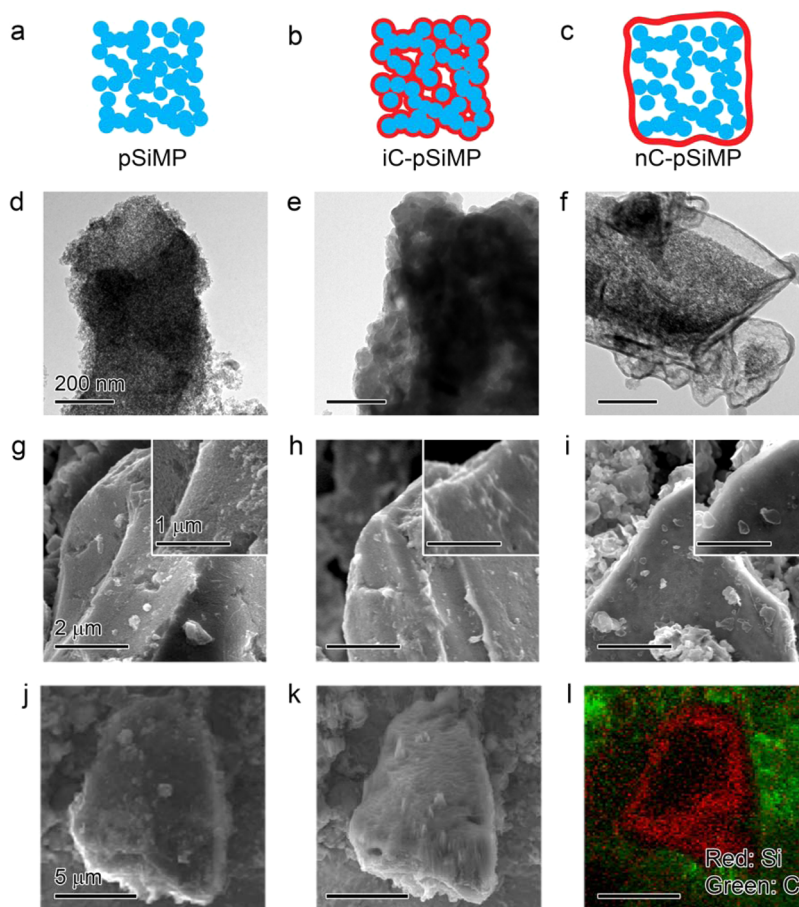
Figure 2. Morphology characterization of pSiMPs with different coatings. Schematic and TEM and SEM images of pSiMPs without coating (a, d, and g), impregnating C-coating (b, e, and h), and nonfilling C-coating (c, f, and i). Insets are magnified SEM images showing the surface of the microparticles. (j—l) Auger electron spectron (AES) elemental mapping of nC-pSiMPs: (j) original sample; (k) after the top surface was removed by Ar ion beam sputtering (5 kV, 5 mA) for 4 min; (l) AES elemental mapping after removing the surface. The majority of C signals are outside the microparticles, showing that very little carbon penetrated into the pore space of the Si microstructures.

the feature of interconnected Si nanoparticles is clearly exhibited again because the carbon layer only wraps the outer layer of the microparticle, as shown in Figure 2f. The SEM images (Figure 2g—i) show that the morphology of the microparticles is stable during the polymer coating, thermal disproportion, and HF etching processes. Auger electron spectroscopy (AES) elemental mapping of the interior of nC-pSiMPs was utilized to further confirm the carbon distribution in the composite structures (Figure 2j—l). After the outer carbon surface was removed by Ar ion beam sputtering (5 kV, 5 mA) for 4 min, only weak carbon signals were observed. This suggests that little carbon penetrates into the interior Si porous structures.

X-ray diffraction (XRD) measurement (Figure 3a) indicates that the nC-pSiMP has a pure silicon phase (JCPDS card No. 27-1402). Calculation with the Debye—Scherrer formula using the strongest peak ($2\theta = 28.5°$) gives a grain size of less than 5 nm for the samples. This is consistent with TEM images showing that the microparticles are composed of silicon nanoparticle domains. Raman spectroscopy (Figure 3b) shows three

peaks at 499, 1340, and 1583 cm^{-1}, corresponding to the silicon and carbon D and G bands, respectively. X-ray photoelectron spectroscopy (XPS, Figure 3c) also demonstrates the coexistence of silicon and carbon. Compared with the carbon, the negligible signal of Si_{2p} in XPS analysis shows a very low surface atomic percentage of Si, clearly indicating that the carbon coating is conformal to completely seal the pSiMPs. The mass percentage of silicon in the nC-pSiMP structure is found to be 89% by thermogravimetric analysis (TGA, Figure 3d), while the percentage decreases to 79% in impregnating coated structure.

A sufficient internal void space is necessary to keep the core—shell structure intact and maintain the structural integrity of the silicon anode. To evaluate whether the void space is enough for the Si expansion or not, we performed an *in situ* TEM study for the nC-pSiMPs with different sizes. The *in situ* electrochemical cell is based on our previous studies and is shown schematically in Figure 4a. Figure 4b demonstrations a series of images taken form a movie of the *in situ* lithiation of the composite with a size of around 500 nm
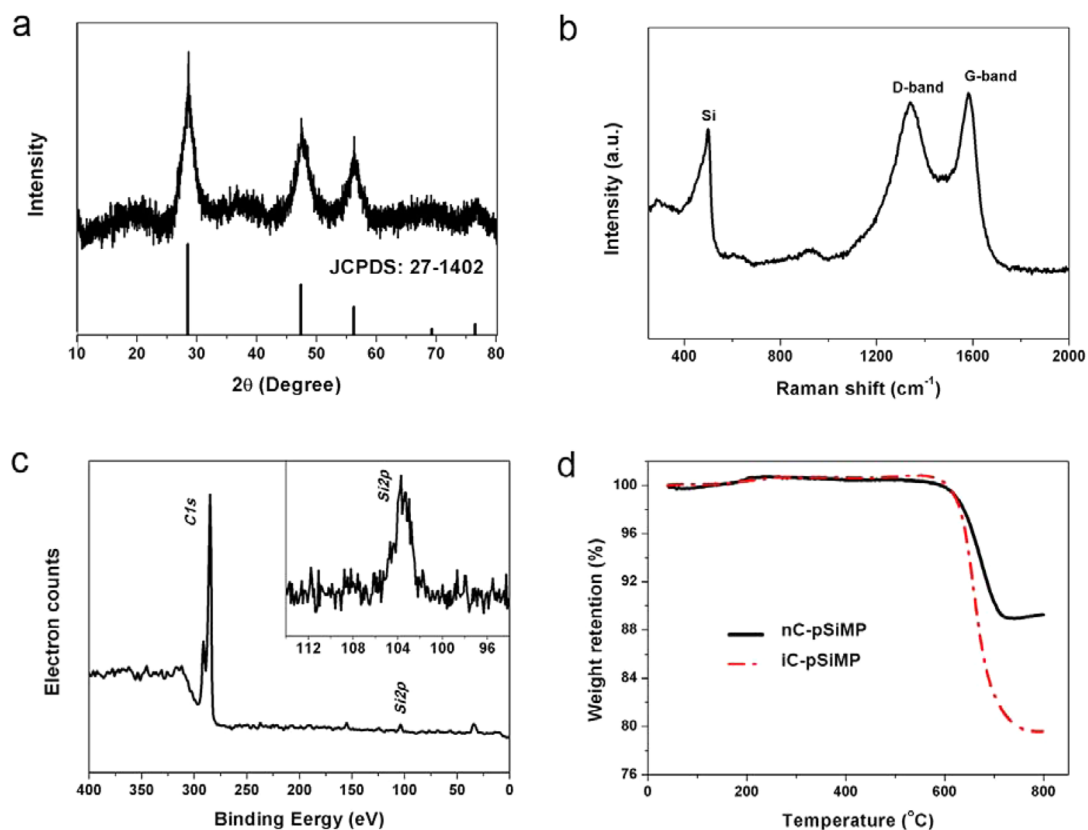
Figure 3. Characterization of nC-pSiMPs. (a) XRD pattern; all the peaks are attributed to crystalline Si. (b) Raman spectrum. (c) XPS spectrum. Inset is a high-resolution XPS spectrum of the Si_{2p} peaks. The signal of Si is significantly low compared with that of carbon, indicating pSiMPs were completely covered by carbon. (d) TGA profiles. The red dashed curve demonstrates the TGA profile of iC-pSiMPs for comparison.
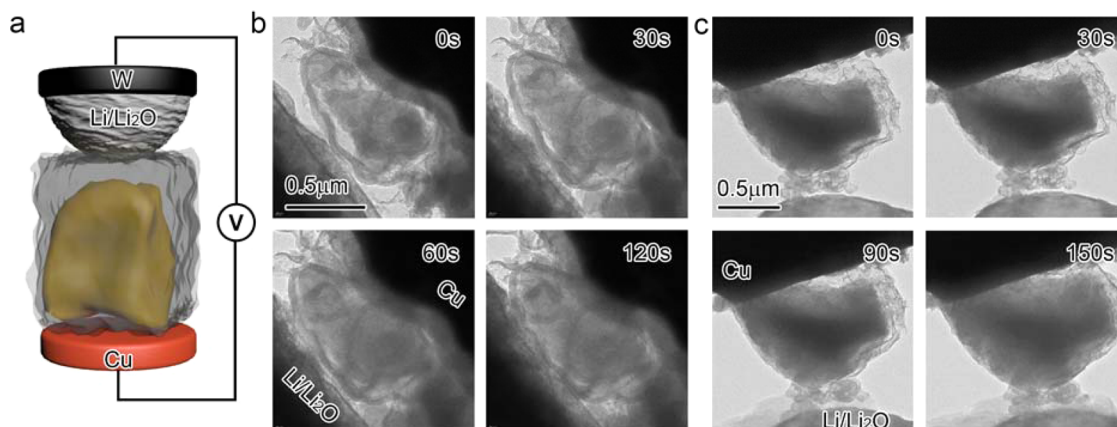

Figure 4. Volume expansion of nC-pSiMPs during lithiation characterized by *in situ* TEM. (a) Schematic of the *in situ* TEM device. (b) Time-lapse images of the lithiation of a 500 nm particle (also see Supplementary Movie S1). Li transports along and across the carbon layer to react with the Si inside, causing volume expansion. Because the pore structure provides enough space to accommodate this expansion, the carbon shell remains intact after full lithiation. (c) Lithiation of a 1 μm nC-pSiMP (also see Supplementary Movie S2).

(Supplementary Movie 1). In the first image (0 s, before lithiation), the porous Si particle is visible within a surrounding C shell. Then, the particle expands in volume as Li diffuses through the carbon layer and alloys with Si. The particle is partially lithiated after 30 s. After 1 min, the contrast inside the carbon shell changes little from TEM images, indicating full lithiation is reached. All the void space is occupied by lithiated silicon material, and no fracture of the carbon shell is observed after full lithiation. For the particle size above 1 μm (Figure 4c, Supplementary Movie 2), more time is needed for the full lithiation (150 s). The porous microsized particle also provides enough void space to accommodate the Si full expansion without rupturing
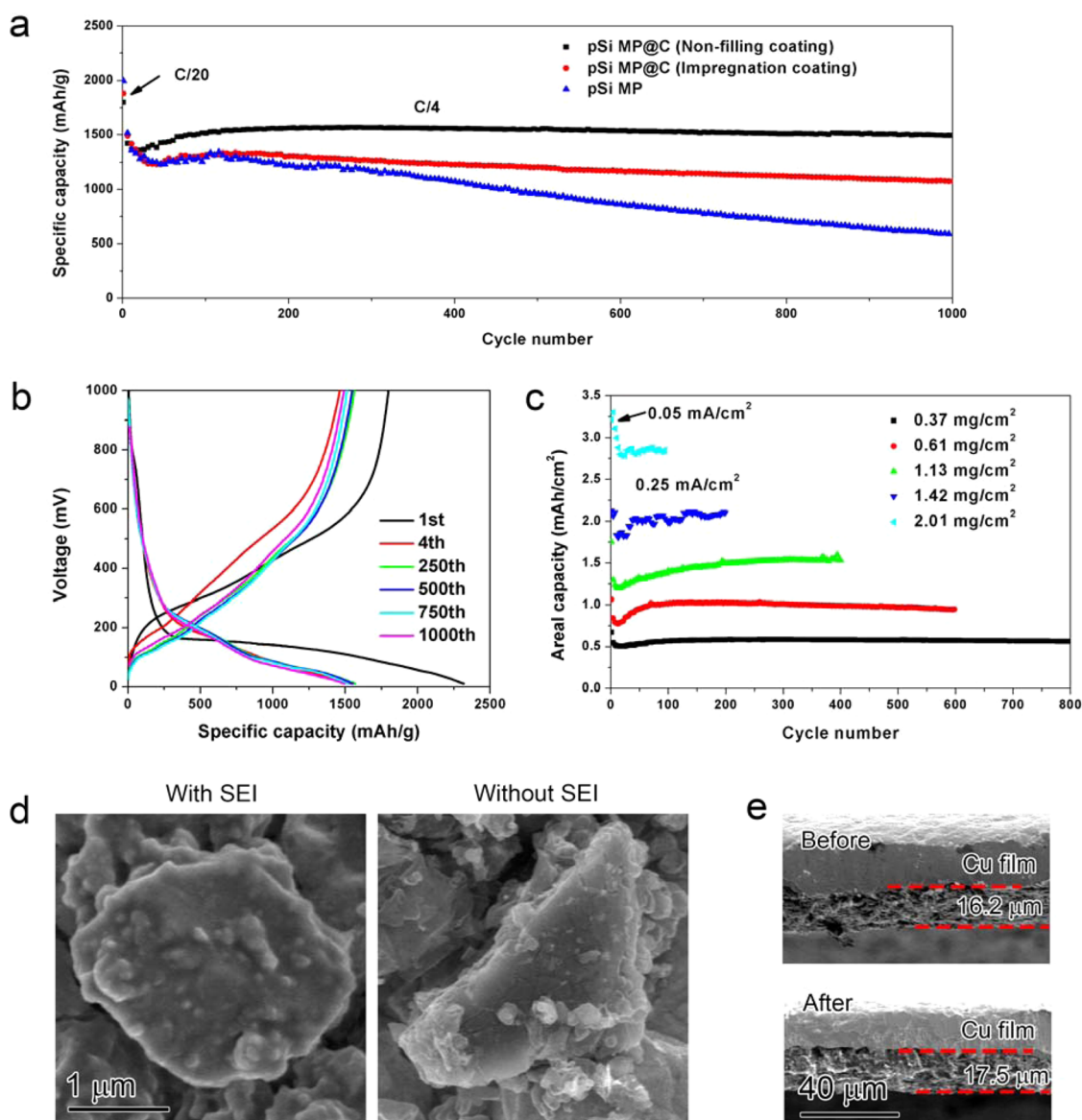
Figure 5. Electrochemical characterization of nC-pSiMP anodes. All the specific capacities of the anodes are based on the total mass of the active materials (Si and C in the nC-pSiMPs). (a) Reversible delithiation capacity for the first 1000 galvanostatic cycles of the pSiMPs with different coating. The active material mass loading was around 0.5 mg cm^{-2}. The rate was C/20 for the first three cycles and then C/4 for later cycles. 1C = 4.2 A g^{-1}. (b) Voltage profiles of nC-pSiMPs plotted for the first, fourth, 250th, 500th, 750th, and 1000th cycles. (c) High areal mass loading test (up to 2.0 mg cm^{-2} active materials) of nC-pSiMPs. All electrodes were cycled at 0.05 mA cm^{-2} for the initial three cycles and 0.25 mA cm^{-2} for later cycles. (d) Typical SEM images of nC-pSiMPs after 100 cycles. The morphologies of SiMPs were largely unchanged compared to those of the original Si samples. (e) Thickness of an nC-pSiMP electrode before cycling and after lithiation to 0.05 V at the 100th cycle.

the outer carbon shell. All these results suggest that without any complex design or sacrificial template our procedure can directly generate a well-defined void space together with a nonfilling coating. This void space is mostly occupied when Si expands in the lithiated state, which maximizes the volumetric capacity. Meanwhile the carbon shell remains intact even after complete Si lithiation, effectively preventing the battery anode from changing structurally upon cycling and thus increasing the cycling life of the battery.

Electrochemical Performance. The electrochemical cycling performance of the composite electrodes was evaluated using deep charge/discharge galvanostatic

cycling from 1 to 0.01 V (Figure 3a–c). As shown in Figure 5a, the initial reversible capacity of nC-SiMPs reaches 1798 mAh g^{-1} for a rate of C/20 (1C = 4.2 A g^{-1} active materials). If not mentioned, all the reported capacities are based on the total mass of Si/C composites. Because the mass percentage of silicon is 89% in the composite, the capacity with respect to silicon is about 2020 mAh g^{-1}. The volumetric capacity for this anode is determined to be 1003 mAh cm^{-3} (based on an areal mass loading of 0.614 mg cm^{-2}, a laminate thickness of 11 μm, and an electrode density of 0.55 g cm^{-3}), which is much larger than the 600 mAh cm^{-3} obtained from state-of-the-art graphite

anodes.[12] From the fourth to 1000th cycle at a rate of C/4, the capacity remains in the range from 1463 to 1560 mAh g^{-1}, and no obvious decay is found. After 1000 cycles, over 1490 mAh g^{-1} capacity remained, which is about 4 times the theoretical capacity of graphite. Under the same conditions, iC-pSiMPs (without an internal void space) demonstrated noticeable decay after 200 cycles. Bare pSiMPs decay even more significantly, with a capacity retention less than 45% after 1000 cycles. The voltage profiles of nC-pSiMPs show the typical electrochemical features of silicon (Figure 5b). The shape of the profiles does not change from the 250th to the 1000th cycle, indicating stable electrochemical behavior of the nonfilling coated structures.

It should be noted that many publications report only specific capacity normalized by the weight of the active materials, and low areal mass loading helps to achieve the stable cycling.[17,44] However, high areal mass loading is necessary for practical batteries. We tested the silicon electrodes with different areal mass loading of composites up to 2.01 mg cm^{-2} (Figure 5c). A reversible areal capacity of 3.22 mAh cm^{-2} is achieved at the first cycle with a current density of 0.05 mA cm^{-2}, corresponding to a specific capacity of 1602 mAh g^{-1} based on the total mass of the Si/C composites. The capacity remains stable during the subsequent fourth to 100th cycles at a higher rate of 0.25 mA cm^{-2}, and the areal capacity is maintained at 2.84 mAh cm^{-2} after 100 cycles, which is close to the capacity of a commercial lithium-ion battery cell. The electrodes with slightly low areal mass loadings of 1.42 and 1.13 mg cm^{-2} offer stable areal capacities of 2.09 and 1.53 mAh cm^{-2}, respectively. Little decrease of specific capacity is found when areal mass loading is increased (1505, 1531, 1359, 1474, and 1413 mAh g^{-1} for the corresponding areal mass loading of 0.37, 0.61, 1.13, 1.42, and 2.01 mg cm^{-2}), confirming the excellent performance of the Si anode originates from the well-designed structures.

DISCUSSION

We attribute the exceptional electrochemical stability to the novel nanoscale architecture of the Si—C composite electrode. The void space generated during the thermal disproportionation and etching process retains secondary particles and stabilizes the SEI on the surface. After 100 deep cycles, the morphology of the nC-pSiMPs with and without SEI was examined under SEM (Figure 5d). The micrometer-sized secondary particle is covered by a thin and uniform SEI layer. An intact carbon shell with silicon inside is clearly shown after removing the SEI with diluted acid. The whole particle is still completely wrapped by carbon. This further suggests the importance of the nonfilling carbon coating on the structural integrity of pSiMPs during the electrochemical cycling. The thickness of

the electrode slightly increases from 16.2 μm to 17.3 μm after 100 deep cycles (Figure 5e). This small volume change (only 8%) guarantees the excellent battery performance in high mass loading cells.

Moreover, the void space is automatically formed through thermal disproportionation of SiO followed by etching away SiO$_2$. According to the chemical equation

$$2SiO \rightarrow Si + SiO_2 \tag{1}$$
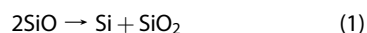
2 mol of SiO will generate 1 mol of Si and 1 mol of SiO$_2$. On the basis of the density of SiO, Si, and SiO$_2$ (2.1, 2.3, and 2.6 g cm^{-3}), we estimate that 1.00 cm^3 of SiO can generate 0.30 cm^3 of Si and 0.55 cm^3 of SiO$_2$ after thermal disproportionation. Therefore, the SiO microparticle will have a volume decrease of 15% after heat treatment, which creates a gap between the silicon particle and carbon shell, as evidenced by the TEM image (Figure 2f). Moreover, the volume ratio of Si to void space is about 3:7 after removing SiO$_2$. This volume ratio allows for free volume expansion of Si materials without breaking the C shell. There is nearly no excess void space when the Si—C composite is fully lithiated, providing a high volumetric energy density. No complex designs or sacrificial templates are needed for this well-defined void space, making the preparation procedure very simple and cost-effective.

The nonfilling C coating not only maintains structural integrity of the secondary particles but also decreases the carbon fraction in composites from 21% to 11% compared with that in the impregnating coating (TGA analysis, Figure 3d). Low carbon content increases the specific capacity of the composite structures. In addition, low carbon content increases the first cycle Coulombic efficiency (CE) because amorphous carbon irreversibly reacts with lithium at low potential. As a result, the first cycle reversible capacity of the nonfilling coated structure reaches 1798 mAh g^{-1} with respect to the total mass of the Si/C composite, while the CE reaches 78%. As a comparison, the impregnating coated structure has a reversible capacity of 1716 mAh g^{-1} with 68% initial CE.

CONCLUSION

In summary, we have designed a nonfilling carbon-coated SiMP structure to address the issues of material fracture and SEI stability in a Si anode. The thermal disproportionation and etching processes provide the interconnected Si nanoparticles sufficient void space for Si expansion, while the nonfilling coated carbon shell maintains the structural integrity of the SiMPs and prevents continuous SEI formation. As a result, the anodes can be deeply cycled up to 1000 times with capacity remaining around 1500 mAh g^{-1}. The areal capacity can reach higher than 3 mAh cm^{-2} without obvious capacity decay after 100 cycles. In addition, the material synthesis and electrode fabrication processes are simple, scalable, highly reproducible, and

compatible with slurry coating manufacturing technology. As a result, the nC-pSiMPs presented here show great promise for future mass production as a high-performance composite anode.

METHODS

Synthesis of nC-pSiMPs. The schematic of the preparation procedure is shown in Supporting Information. Commercial silicon monoxide microparticles (SiO MPs, 325 mesh) were first coated with a resorcinol-formaldehyde resin layer. The RF was then converted into a carbon layer under argon at 950 °C for 5 h. During this annealing process, SiO MPs phase separate to form a Si/SiO$_2$ composite with interconnected Si nanoparticles embedded in a SiO$_2$ matrix due to the disproportionation of SiO. Finally, the SiO$_2$ matrix was removed with 10 wt % HF solution to form the final product, nC-pSiMPs. For the bare porous structure without C coating, SiO was directly heated to 950 °C under the same conditions and then SiO$_2$ was removed with HF. Impregnating coated samples could be achieved by coating RF on these bare pSiMPs followed by a carbonization process.

Characterization. The weight percentage of Si and C in the C-coated pSiMPs was determined from the weight loss curves measured under simulated air atmosphere (20% O$_2$ + 80% Ar, both are ultrapurity grade gases from Airgas) on a TG/DTA Instruments Netzsch STA 449 with a heating rate of 5 °C/min. SEM and TEM images were taken using a FEI XL30 Sirion SEM (accelerating voltage 5 kV) and a FEI Tecnai G2 F20 X-TWIN (accelerating voltage 200 kV), respectively. Other characterization was carried out by X-ray photoelectron spectroscopy (PHI Versa Probe 5000, Physical Electronics, USA), X-ray diffraction (PANalytical X'Pert, Ni-filtered Cu Kα radiation), and Raman spectroscopy (531 nm excitation laser, WITEC Raman spectrometer).

***In Situ* TEM.** A specialized dual-probe electrical biasing holder (Nanofactory 105 Instruments) was used. By biasing the working electrode between −2.5 and −3 V *versus* the counter electrode, Li$^+$ ions flow through the lithium oxide/nitride layer and are reduced at the working electrode, where they react with carbon and alloy with the silicon in the coated structures (Figure 4a). The lithiation time of the C-coated porous structures is less than 3 min (Figure 4b,c).

Electrochemical Mearsurement. To prepare the working electrodes, the various pSiMPs were mixed with carbon black (Super P) and polyvinylidene fluoride binder (80:10:10 by weight) in *N*-methyl-2-pyrrolidinone to form a slurry. This slurry was then coated onto copper foil using a doctor blade and dried under vacuum to form the working electrode. Coin cells (2032-type) were assembled in an argon-filled glovebox using lithium foil as the counter electrode. The electrolyte was 1.0 M LiPF$_6$ in 1:1 w/w ethylene carbonate/diethyl carbonate, with 1 vol % vinylene carbonate added to improve the cycling stability. All the cells were cycled between 0.01 and 1 V *versus* Li/Li$^+$. Specific capacity values were calculated based on the total mass of the Si/C composite structures.

Conflict of Interest: The authors declare no competing financial interest.

Supporting Information Available: More detailed synthesis procedures, additional SEM images, Coulombic efficiency, and *in situ* TEM movies are available free of charge *via* the Internet at http://pubs.acs.org.

REFERENCES AND NOTES

1. Arico, A. S.; Bruce, P.; Scrosati, B.; Tarascon, J.-M.; van Schalkwijk, W. Nanostructured Materials for Advanced Energy Conversion and Storage Devices. *Nat. Mater.* **2005**, *4*, 366–377.
2. Armand, M.; Tarascon, J. M. Building Better Batteries. *Nature* **2008**, *451*, 652–657.
3. Bruce, P. G.; Freunberger, S. A.; Hardwick, L. J.; Tarascon, J.-M. Li-O$_2$ and Li-S Batteries with High Energy Storage. *Nat. Mater.* **2012**, *11*, 19–29.
4. Dunn, B.; Kamath, H.; Tarascon, J.-M. Electrical Energy Storage for the Grid: A Battery of Choices. *Science* **2011**, *334*, 928–935.
5. Chen, Z.; Qin, Y.; Amine, K.; Sun, Y. K. Role of Surface Coating on Cathode Materials for Lithium-Ion Batteries. *J. Mater. Chem.* **2010**, *20*, 7606–7612.
6. Sun, Y.-K.; Myung, S.-T.; Park, B.-C.; Prakash, J.; Belharouak, I.; Amine, K. High-Energy Cathode Material for Long-Life and Safe Lithium Batteries. *Nat. Mater.* **2009**, *8*, 320–324.
7. Wang, J.; Yang, J.; Tang, Y.; Liu, J.; Zhang, Y.; Liang, G.; Gauthier, M.; Karen Chen-Wiegart, Y.-c.; Norouzi Banis, M.; Li, X., *et al.* Size-Dependent Surface Phase Change of Lithium Iron Phosphate during Carbon Coating. *Nat. Commun.* **2014**, *5*, 4415.
8. Wei Seh, Z.; Li, W.; Cha, J. J.; Zheng, G.; Yang, Y.; McDowell, M. T.; Hsu, P.-C.; Cui, Y. Sulphur−TiO$_2$ Yolk−Shell Nanoarchitecture with Internal Void Space for Long-Cycle Lithium−Sulphur Batteries. *Nat. Commun.* **2013**, *4*, 1331.
9. Beaulieu, L. Y.; Eberman, K. W.; Turner, R. L.; Krause, L. J.; Dahn, J. R. Colossal Reversible Volume Changes in Lithium Alloys. *Electrochem. Solid-State Lett.* **2001**, *4*, A137–A140.
10. Deshpande, R.; Cheng, Y.-T.; Verbrugge, M. W. Modeling Diffusion-Induced Stress in Nanowire Electrode Structures. *J. Power Sources* **2010**, *195*, 5081–5088.
11. Obrovac, M. N.; Christensen, L. Structural Changes in Silicon Anodes during Lithium Insertion/Extraction. *Electrochem. Solid-State Lett.* **2004**, *7*, A93–A96.
12. Obrovac, M. N.; Christensen, L.; Le, D. B.; Dahn, J. R. Alloy Design for Lithium-Ion Battery Anodes. *J. Electrochem. Soc.* **2007**, *154*, A849–A855.
13. Aurbach, D. Review of Selected Electrode−Solution Interactions Which Determine the Performance of Li and Li Ion Batteries. *J. Power Sources* **2000**, *89*, 206–218.
14. Chan, C. K.; Ruffo, R.; Hong, S. S.; Cui, Y. Surface Chemistry and Morphology of the Solid Electrolyte Interphase on Silicon Nanowire Lithium-Ion Battery Anodes. *J. Power Sources* **2009**, *189*, 1132–1140.
15. Verma, P.; Maire, P.; Novák, P. A Review of the Features and Analyses of the Solid Electrolyte Interphase in Li-Ion Batteries. *Electrochim. Acta* **2010**, *55*, 6332–6341.
16. Obrovac, M. N.; Chevrier, V. L. Alloy Negative Electrodes for Li-Ion Batteries. *Chem. Rev.* **2014**, *114*, 11444–11502.
17. Wu, H.; Chan, G.; Choi, J. W.; Ryu, I.; Yao, Y.; McDowell, M. T.; Lee, S. W.; Jackson, A.; Yang, Y.; Hu, L.; *et al.* Stable Cycling of Double-Walled Silicon Nanotube Battery Anodes through Solid-Electrolyte Interphase Control. *Nat. Nanotechnol.* **2012**, *7*, 310–315.
18. Liu, N.; Wu, H.; McDowell, M. T.; Yao, Y.; Wang, C.; Cui, Y. A Yolk-Shell Design for Stabilized and Scalable Li-Ion Battery Alloy Anodes. *Nano Lett.* **2012**, *12*, 3315–3321.
19. Wu, H.; Zheng, G.; Liu, N.; Carney, T. J.; Yang, Y.; Cui, Y. Engineering Empty Space between Si Nanoparticles for Lithium-Ion Battery Anodes. *Nano Lett.* **2012**, *12*, 904–909.
20. Li, X.; Gu, M.; Hu, S.; Kennard, R.; Yan, P.; Chen, X.; Wang, C.; Sailor, M. J.; Zhang, J.-G.; Liu, J. Mesoporous Silicon Sponge as an Anti-Pulverization Structure for High-Performance Lithium-Ion Battery Anodes. *Nat. Commun.* **2014**, *5*, 5105.

21. Wang, B.; Li, X.; Zhang, X.; Luo, B.; Zhang, Y.; Zhi, L. Contact-Engineered and Void-Involved Silicon/Carbon Nano-hybrids as Lithium-Ion-Battery Anodes. *Adv. Mater.* **2013**, *25*, 3560–3565.

22. Liu, N.; Lu, Z.; Zhao, J.; McDowell, M. T.; Lee, H.-W.; Zhao, W.; Cui, Y. A Pomegranate-Inspired Nanoscale Design for Large-Volume-Change Lithium Battery Anodes. *Nat. Nanotechnol.* **2014**, *9*, 187–192.

23. Chan, C. K.; Peng, H.; Liu, G.; McIlwrath, K.; Zhang, X. F.; Huggins, R. A.; Cui, Y. High-Performance Lithium Battery Anodes Using Silicon Nanowires. *Nat. Nanotechnol.* **2008**, *3*, 31–35.

24. Liu, G.; Xun, S.; Vukmirovic, N.; Song, X.; Olalde-Velasco, P.; Zheng, H.; Battaglia, V. S.; Wang, L.; Yang, W. Polymers with Tailored Electronic Structure for High Capacity Lithium Battery Electrodes. *Adv. Mater.* **2011**, *23*, 4679–4683.

25. Magasinski, A.; Dixon, P.; Hertzberg, B.; Kvit, A.; Ayala, J.; Yushin, G. High-Performance Lithium-Ion Anodes Using a Hierarchical Bottom-up Approach. *Nat. Mater.* **2010**, *9*, 353–358.

26. Park, M.-H.; Kim, M. G.; Joo, J.; Kim, K.; Kim, J.; Ahn, S.; Cui, Y.; Cho, J. Silicon Nanotube Battery Anodes. *Nano Lett.* **2009**, *9*, 3844–3847.

27. Wu, H.; Cui, Y. Designing Nanostructured Si Anodes for High Energy Lithium Ion Batteries. *Nano Today* **2012**, *7*, 414–429.

28. Evanoff, K.; Magasinski, A.; Yang, J.; Yushin, G. Nanosilicon-Coated Graphene Granules as Anodes for Li-Ion Batteries. *Adv. Energy Mater.* **2011**, *1*, 495–498.

29. Xu, Y.; Liu, Q.; Zhu, Y.; Liu, Y.; Langrock, A.; Zachariah, M. R.; Wang, C. Uniform Nano-Sn/C Composite Anodes for Lithium Ion Batteries. *Nano Lett.* **2013**, *13*, 470–474.

30. Bang, B. M.; Lee, J.-I.; Kim, H.; Cho, J.; Park, S. High-Performance Macroporous Bulk Silicon Anodes Synthesized by Template-Free Chemical Etching. *Adv. Energy Mater.* **2012**, *2*, 878–883.

31. Thakur, M.; Sinsabaugh, S. L.; Isaacson, M. J.; Wong, M. S.; Biswal, S. L. Inexpensive Method for Producing Macro-porous Silicon Particulates (MPSPs) with Pyrolyzed Poly-acrylonitrile for Lithium Ion Batteries. *Sci. Rep.* **2012**, *2*, 795.

32. Ge, M.; Rong, J.; Fang, X.; Zhou, C. Porous Doped Silicon Nanowires for Lithium Ion Battery Anode with Long Cycle Life. *Nano Lett.* **2012**, *12*, 2318–2323.

33. Jung, D. S.; Hwang, T. H.; Park, S. B.; Choi, J. W. Spray Drying Method for Large-Scale and High-Performance Silicon Negative Electrodes in Li-Ion Batteries. *Nano Lett.* **2013**, *13*, 2092–2097.

34. Kim, H.; Cho, J. Superior Lithium Electroactive Mesoporous Si@Carbon Core−Shell Nanowires for Lithium Battery Anode Material. *Nano Lett.* **2008**, *8*, 3688–3691.

35. Kim, H.; Han, B.; Choo, J.; Cho, J. Three-Dimensional Porous Silicon Particles for Use in High-Performance Lithium Secondary Batteries. *Angew. Chem., Int. Ed.* **2008**, *47*, 10151–10154.

36. Yi, R.; Dai, F.; Gordin, M. L.; Chen, S.; Wang, D. Micro-Sized Si-C Composite with Interconnected Nanoscale Building Blocks as High-Performance Anodes for Practical Application in Lithium-Ion Batteries. *Adv. Energy Mater.* **2013**, *3*, 295–300.

37. Song, J.; Chen, S.; Zhou, M.; Xu, T.; Lv, D.; Gordin, M. L.; Long, T.; Melnyk, M.; Wang, D. Micro-Sized Silicon-Carbon Composites Composed of Carbon-Coated Sub-10 nm Si Primary Particles as High-Performance Anode Materials for Lithium-Ion Batteries. *J. Mater. Chem. A* **2014**, *2*, 1257–1262.

38. Lee, J.-I.; Choi, N.-S.; Park, S. Highly Stable Si-Based Multi-component Anodes for Practical Use in Lithium-Ion Batteries. *Energy Environ. Sci.* **2012**, *5*, 7878–7882.

39. Lee, J.-I.; Lee, K. T.; Cho, J.; Kim, J.; Choi, N.-S.; Park, S. Chemical-Assisted Thermal Disproportionation of Porous Silicon Monoxide into Silicon-Based Multicomponent Systems. *Angew. Chem., Int. Ed.* **2012**, *51*, 2767–2771.

40. Yi, R.; Dai, F.; Gordin, M. L.; Sohn, H.; Wang, D. Influence of Silicon Nanoscale Building Blocks Size and Carbon Coating on the Performance of Micro-Sized Si−C Composite Li-Ion Anodes. *Adv. Energy Mater.* **2013**, *3*, 1507–1515.

41. Liu, X. H.; Zhong, L.; Huang, S.; Mao, S. X.; Zhu, T.; Huang, J. Y. Size-Dependent Fracture of Silicon Nanoparticles during Lithiation. *ACS Nano* **2012**, *6*, 1522–1531.

42. McDowell, M. T.; Ryu, I.; Lee, S. W.; Wang, C.; Nix, W. D.; Cui, Y. Studying the Kinetics of Crystalline Silicon Nanoparticle Lithiation with in Situ Transmission Electron Microscopy. *Adv. Mater.* **2012**, *24*, 6034–6041.

43. Li, N.; Zhang, Q.; Liu, J.; Joo, J.; Lee, A.; Gan, Y.; Yin, Y. Sol-Gel Coating of Inorganic Nanostructures with Resorcinol-Formaldehyde Resin. *Chem. Commun.* **2013**, *49*, 5135–5137.

44. Gogotsi, Y.; Simon, P. True Performance Metrics in Electro-chemical Energy Storage. *Science* **2011**, *334*, 917–918.